Available online at www.sciencedirect.com
SCIENCE DIRECT®
Remote Sensing of Environment 103 (2006) 236–245
Remote Sensing of Environment
www.elsevier.com/locate/rse

A multi-angle spectrometer for automatic measurement of plant canopy reflectance spectra

Ray Leuning [a,*], Dale Hughes [a], Paul Daniel [b], Nicholas C. Coops [d], Glenn Newnham [c]

[a] CSIRO Atmospheric Research, P.O. Box 1666 Canberra, ACT 2601 Australia
[b] CSIRO Land and Water, P.O. Box 1666 Canberra, ACT 2601 Australia
[c] ENSIS, Private Bag 10, Clayton South, Vic. 3169 Australia
[d] Department of Forest Resource Management, Forest Sciences Centre, 2424 Main Mall, University of British Columbia, Vancouver, BC, Canada V6T 1Z4

Received 13 April 2004; received in revised form 29 June 2005; accepted 30 June 2005

Abstract

The paper describes the design and operation of a multi-angle spectrometer (MAS) for automatic measurement of near-field spectral reflectances of plant canopies at hourly intervals. A novel feature of the instrument is a rotating periscope connected to a spectrometer via a fiber optic cable. Canopy reflectances are calculated for multiple view azimuths, at a single zenith angle from measurements of spectrometer dark current, incoming solar irradiance and reflected radiances. Spectral measurements are made between 300 and 1150 nm wavelength at a band-to-band spacing of 3 nm, and a bandwidth (full-width, half maximum) of 10 nm. Preliminary data analysis showed that the canopy reflectance model of Kuusk [Kuusk, A. (1995). A fast, invertible canopy reflectance model. *Remote Sensing of Environment* 51, 342–350] reproduced the observed large differences in visible and near-infrared (NIR) reflectances, but the model was unable to predict quantitatively the observed variations in the measured reflectance spectra with azimuth, particularly in the NIR. Discrepancies between model and measurements are likely due to the inhomogeneous nature of the forest canopy in contrast to the assumption of a uniformly absorbing turbid medium in the model. Measurements using the MAS can be used to investigate directional dependences of reflectance indices and for testing BRDF models used to separate geometrical and plant physiological contributions to the reflectance signals. The MAS provides continuous sampling of reflectance indices which can be compared with canopy properties such as chlorophyll content and photosynthetic capacity.

Keywords: Hyperspectral radiometer; Periscope; Plant canopy reflectance, Spectral reflectance indices

1. Introduction

Remote sensing offers the possibility of monitoring the carbon and water cycles over multiple time and space scales. Goward et al. (1985) provided an early example of using remotely sensed data to estimate gross- and net-primary production as a function of the Normalized Difference Vegetation Index (NDVI). This index is a function of surface reflectance in the visible and near-infrared (NIR) portions of the solar spectrum and is linearly related to the amount of photosynthetically active radiation absorbed by green vegetation (A_{PAR}). Gross primary production (GPP) is estimated by the product $A_{PAR}R_{UE}$, where R_{UE} is the radiation-use efficiency of the vegetation (Goward et al., 1985; Monteith, 1977). To date, R_{UE} has been derived from ecophysiological studies rather than through remote sensing, but work by Gamon et al. (1997, 2001), Hanan et al. (1995), Peñuelas et al. (1995), Prince (1991), and Waring et al. (1995), has shown strong correlations between R_{UE} and indices derived from various remote-sensing systems. Remote sensing has also been combined with mechanistic models of photosynthesis (Sellers et al., 1992), through estimates of leaf area index (L_{AI}), leaf nitrogen content and photosynthetic capacity (Boegh et al., 2002; Carter, 1998). Remotely sensed reflectance spectra thus offer the possibility of estimating the spatial variation in various canopy properties such as R_{UE}, A_{PAR}, L_{AI}, leaf nitrogen and chlorophyll contents and photosynthetic capacity.

Canopy reflectances are now measured by a variety of sensors mounted on aircraft and satellites. Hyperspectral data

* Corresponding author. Tel.: +61 2 62465557.
E-mail address: ray.leuning@csiro.au (R. Leuning).

0034-4257/$ - see front matter © 2006 Elsevier Inc. All rights reserved.
doi:10.1016/j.rse.2005.06.016

are available from airborne systems such as AVIRIS (Advanced Visible Infrared Imaging Spectrometer; NASA JPL), CASI (Compact Airborne Spectrographic Imager; ITRES, 1989) and HyMap® (HyVista Corporation, 2000), and from the space-borne sensor, Hyperion on EO-1 (Pearlman et al., 2003). Reflectance data in a smaller number of wavebands are also available globally from the Moderate Resolution Imaging Spectrometers (MODIS) on the Aqua and Terra satellites (http://modis.gsfc.nasa.gov/about/index.html). Spectral reflectance measurements from each of these instruments may be useful in estimating R_{UE} and other plant canopy properties, but before this potential can be realized, relationships established between reflectance spectra, R_{UE} and photosynthetic capacity at the leaf level must be extended to plant canopies. Combining hyperspectral reflectance measurements with data from the global network of flux stations (Baldocchi et al., 2001; Running et al., 1999) provides an ideal opportunity for developing such relationships, but there remains the problem of a mismatch in spatial and temporal scales between remotely sensed observations and flux measurements. For example, MODIS radiances are measured twice daily, at a spatial resolution of 250 m in the red and near infrared wavebands, and at 500 m resolution in five other bands, whereas fluxes are measured continuously for areas typically 500–1000 m radius. An approach to resolving these scaling issues lies with the newly developed SpecNet initiative (Gamon et al., 2006-this issue). SpecNet complements the existing FLUXNET network of micrometeorological flux stations and promotes the installation of spectrometers on tower sites to measure near-surface spectra at time and space scales similar to those of the flux towers. A key objective is to use the reflectance and flux measurements to develop and test relationships between canopy properties and various reflectance indices at the local scale. One possibility is to use the flux measurements to estimate photosynthetic capacity in a land-surface scheme (Wang et al., 2001), and then to use remotely sensed reflectances to determine the spatial distribution of photosynthetic capacity in the land-surface scheme (Boegh et al., 2002).

As part of the SpecNet initiative, this paper describes in detail a novel optical periscope that is combined with a spectrometer to measure the spectral reflectance of a forest canopy at four azimuths at hourly intervals every day of the year. The high temporal resolution of the new instrument, known as the multi-angle spectrometer (MAS), complements the twice-daily spectral information available from MODIS. The MAS was designed to view the canopy in several azimuths because there is almost as much information in the directional reflectances as in the spectra themselves when used to infer canopy properties from radiative transfer models (Bicheron & Leroy, 1999). The MAS has been installed on top of a 70-m tower at the Tumbarumba flux station, which is located in a 40-m-tall, evergreen *Eucalyptus* forest in southeast New South Wales, Australia (Leuning et al., 2005). The paper discusses the theory of measuring reflectances with the instrument and data quality-control procedures before presenting examples of irradiance and reflectance spectra measured over the forest. This is followed by a preliminary comparison of the reflectance spectra measured by the MAS with predictions of the model by Kuusk (1995, K 95 model hereafter) for radiation transfer in plant canopies. A key objective is to examine whether the model can quantify the effect of sun and viewing geometry on the measured spectra and hence provide a means to normalize spectra to a standard, zenith view angle. If successful, the normalized spectra could then be used to develop a set of spectral indices for correlation with CO_2 fluxes measured by the eddy covariance technique, or to provide relationships with key canopy properties such as photosynthetic capacity and leaf nitrogen content (e.g., Bicheron & Leroy, 1999).

2. Description of the optical assembly

The MAS consists of two major components: an optical 'periscope' mounted on top of the mast and a Unispec spectrometer (PP Systems, Haverhill, MA, USA) and associated electronics mounted 2 m below the periscope and connected to it via electrical and fiber-optic cables. The spectrometer uses a 256-pixel detector array operating over the spectral range 300 nm to 1150 nm, resulting in a band-to-band spacing of 3 nm, and a bandwidth (full-width, half maximum) of 10 nm.

Fig. 1 shows the mechanical details of the upper enclosure and rotating periscope that samples incoming radiation and radiation reflected from the forest canopy in the selected azimuth directions. The periscope box houses a moveable mirror, shutter and associated electronics and is mounted on a vertical shaft which is turned by a stepper motor mounted in the box beneath the rotating optical assembly. A 600-μm-diameter silicon optical fiber passes through the central support shaft of the periscope and is positioned on the optical axis of the mirror system to collect light for transmission to the spectrometer.

On top of the periscope is a cosine-corrected hemispherical diffuser to sample incoming irradiance. The diffuser material is opal glass with a polished, domed upper surface that resists soiling caused by airborne dust deposition and is self-cleaning during rain. The dome is also manually cleaned periodically. Beneath the diffuser is a mirror mounted at an angle of 45° to the horizon on a small translation stage, and whose position determines whether radiation is sampled from the sky or the canopy. The translation stage is driven via a lead screw and a small DC motor; at each end of the translation stage is a micro-switch that stops the motor when the stage reaches the required position. The periscope assembly performs three functions:

1. Measurement of the detector dark current by closing off all external light. The dark current is subtracted from the other spectral signals before they undergo further processing. In this case the main shutter is closed and the mirror is moved to the 'home' position that blocks the sky port (Fig. 2a). The shutter consists of a spring-loaded vane, activated by a solenoid, that rotates through an angle of approximately 90°. The vane is painted black and has a layer of black felt attached to the underside to exclude light when the shutter is in the closed position.
2. Measurement of the irradiance incident on the canopy via a cosine-corrected hemispherical diffuser. In this case the main

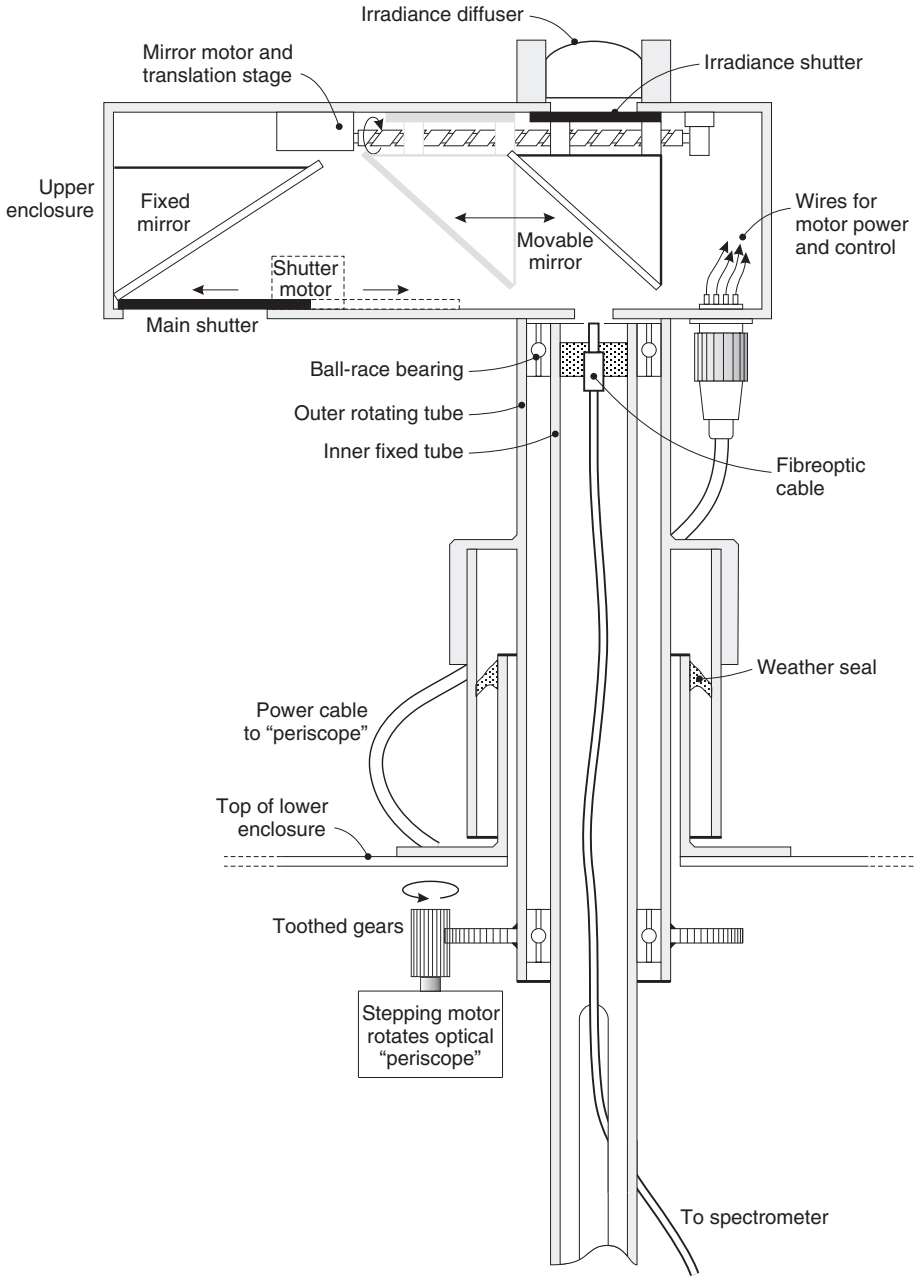

Fig. 1. Mechanical and optical details of the rotating periscope.

shutter is closed and the mirror is positioned so that light passing through the diffuser is sampled by the optical fiber for transmission to the spectrometer (Fig. 2b).

3. Measurement of reflected radiances at four azimuths and at one zenith angle (see Table 1 for values in the two configurations used to date). The moveable mirror in the periscope is positioned so that the sky port is blocked and light from the main aperture is reflected onto the optical fiber field of view. The main shutter is open at this time (Fig. 2c). An index ring at the end of the rotating tube (Fig. 1) determines the azimuth of the optical assembly. Notches cut into the ring allow micro-switches and controlling software to stop the stepper motor at the positions required for the four azimuth directions. The view zenith angle was set initially to 30° but this was subsequently increased to 58° (Table 1), since this angle not only increases the area of canopy sampled, but reduces sensitivity of the reflectance measurements to variations in foliage angle distribution (Lang, 1986, 1987; Warren Wilson, 1960). With the MAS having a ±5° field of view and mounted on a 70-m mast viewing a 40-m tall forest, the area sampled at canopy top is approximately 7 m in the radial direction and 3 m in the azimuth direction for the 30° zenith angle. This increases to approximately 19 m by 8 m at a zenith angle of 58°. The distance from the mast to the canopy sampled is 23 m and 48 m for the two zenith angles, respectively, and there is no

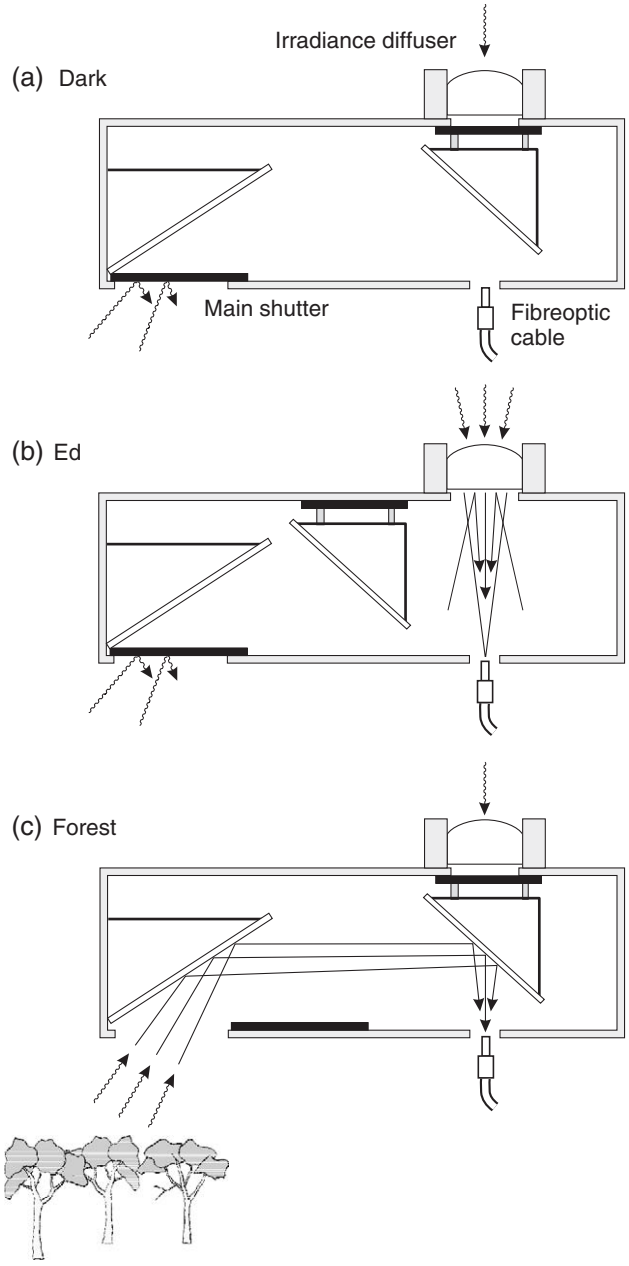

Fig. 2. Mirror and shutter positions for each measurement mode: (a) mirror in home position and shutter closed for measurement of dark current, N_0; (b) moveable mirror in position for measurement of incoming irradiance, E_d; and (c) moveable mirror in place to measure reflected radiance from forest canopy, L_t.

overlap in the areas sampled by the MAS at the four azimuths.

Complete technical details of the optics, electronic control circuitry and data acquisition software can be found in the report by Hughes et al. (2004) available from the authors.

3. Theory of reflectance measurements using the MAS

Consider the measurement of incident irradiance, E_d, using a cosine-corrected hemispherical diffuser (CCHD) mounted on the top surface of the instrument. In this location the CCHD has an unobstructed view of the sky. Some of the incident radiation passes into the diffuser where it is absorbed and scattered within the opal glass matrix, and a fraction d, of E_d is emitted at its lower surface as shown in Fig. 2b. The optical fiber samples this radiation and passes it to the spectrometer, resulting in an instrument reading, N_d, for each waveband. After subtracting the dark current, N_0, the relationship between $N_d - N_0$ and E_d is

$$N_d - N_0 = d\ g_{\mathrm{d}} E_d, \tag{1}$$

where the wavelength dependence of each term in this equation is implicit. The term g_{d} is the gain function of the optical fiber/spectrometer system for downwelling irradiance and accounts for factors such as fiber optic transmission, detector conversion efficiency, integration time and electrical gain.

Now consider the measurement of target radiance. A fraction m of the upwelling radiation from the forest canopy, L_t, is reflected from the two mirrors in the periscope into the optical fiber, before passing to the radiometer (Fig. 2c). This yields an instrument reading, N_t, proportional to the canopy target radiance:

$$N_t - N_0 = g_{\mathrm{u}} m L_t \tag{2}$$

where g_{u} is the gain function for the periscope and optical fiber/spectrometer system during the upward radiance measurement, and where N_t has again been corrected for the instrument dark current reading.

Canopy reflectance, R_t, can now be calculated from the measurements of E_d and L_t using the definition

$$R_t = \frac{L_t}{L_p} = \frac{\pi L_t}{E_d} \tag{3}$$

where L_p is the radiance that would be measured when viewing a theoretical, perfect Lambertian reference panel under the same irradiance E_d that illuminates the forest canopy. Combining (1)–(3) gives

$$R_t = \left(\frac{N_t - N_0}{N_d - N_0}\right)\left(\frac{g_{\mathrm{d}}}{g_{\mathrm{u}}}\right)\frac{\pi d}{m}. \tag{4}$$

Ideally, the gain functions of the instrument, g_{d} and g_{u}, will remain constant with time, but in practice there are small changes in these values associated with changes in temperature, supply voltage, accumulation of dust on the optics and aging of the detector in the spectrometer. However, the same optical fiber

Table 1
Zenith angles and azimuths (degrees) used at Tumbarumba

	Original configuration (18 June 2002–23 September 2003)	Current configuration (5 November 2003–now)
Zenith angle	30	58
Azimuth 1	80	200 (‘W’)
Azimuth 2	350	110 (‘E’)
Azimuth 3	260	20 (‘N’)
Azimuth 4	170	290 (‘S’)

The zenith angle is measured from the vertical and azimuth is relative to the true north.

and spectrometer combination and spectrometer integration times are used for both E_d and L_t measurements. The suite of dark, irradiance and canopy radiance measurements takes approximately 1 min to complete and hence any time-related changes to the instrument will be small over this period. Under these conditions $g_d = g_u$, and hence, explicit knowledge of g_d and g_u is not required. Thus, (4) reduces to

$$R_t = \left(\frac{N_t - N_0}{N_d - N_0}\right)\frac{\pi d}{m}. \quad (5)$$

This equation shows that the reflectance can be calculated from N_t and N_d once the dark current reading and the ratio d/m is known, which relates the different sensitivities between the E_d and L_t optical pathways.

Instrument calibration is done by taking near-simultaneous measurements of E_d and the radiance from a reference panel of known reflectance, R_{ref}, where the irradiance illuminating the panel is also E_d. In this case

$$\frac{\pi d}{m} = R_{ref}\left(\frac{N_{dp} - N_{0p}}{N_{tp} - N_{0p}}\right), \quad (6)$$

where the added subscript p indicates calibration measurements performed using a reference panel. Values of spectral reflectance R_{ref} for the Spectralon SRT-990 reference panel used in the calibration were supplied by the manufacturer (Labsphere, Inc., North Sutton, NH, USA). Calibration of the system was performed at solar noon during a clear, sunny day when E_d remained essentially constant. This allows calculation of R_t using

$$R_t(\lambda) = \left[\frac{N_t(\lambda) - N_0(\lambda)}{N_d(\lambda) - N_0(\lambda)}\right] R_{ref}(\lambda) \left[\frac{N_{dp}(\lambda) - N_{0p}(\lambda)}{N_{tp}(\lambda) - N_{0p}(\lambda)}\right], \quad (7)$$

where the wavelength dependence of each quantity is stated explicitly. In this equation $R_t(\lambda)$ is the calibrated target reflectance, $N_t(\lambda)$, $N_d(\lambda)$, $N_{dp}(\lambda)$, $N_{tp}(\lambda)$ and $N_0(\lambda)$ are the respective MAS readings from measurements of (1) the canopy target radiance, (2) incident irradiance, (3) irradiance during calibration, (4) the radiance from the panel during calibration, and (5) the dark current.

4. Data selection and analysis

Using a custom-built computer interface, the user can select the spectrometer integration time and the number of scans over which the spectra are averaged. A 200-ms integration time is used and 10 scans are averaged at each measurement position (dark current, incoming irradiance and reflected radiances at four azimuths). MAS measurements are made every hour from 0600 to 1800 h, inclusive, although the measurement frequency and daily sampling period are programmable. Data obtained by the MAS are stored on a field computer and at the end of each day the data are transferred automatically via a dial-up modem to a laboratory computer for subsequent analysis.

Poor-quality reflectances are obtained if clouds, rain or fog cause variable irradiance during the 5 min when measurements are being taken by the MAS. The first stage of data quality control involves comparing spectra from each direction with each other to check for any obvious errors arising from mis-positioning of the periscope. Secondly, the measured atmospheric irradiances are compared to a normalized spectral template obtained under clear sky conditions. Peak irradiance (at ~580 nm) is used as the normalizing factor for each measurement period. The analysis software allows the user to select an envelope into which the spectra should fit (currently ±10%); those that do not fit are identified by a flag in the data file, while acceptable spectra are used to compute a number of reflectance indices as described below. A smaller subset of data obtained on totally clear days was used to examine the ability of the K95 model to account for BRDF effects in the observed reflectance spectra. Clear days were identified using measurements from a pyranometer (CM-11, Kipp and Zonen, Delft, The Netherlands). No attempt has been made to fill gaps in the data because data from the instrument will be used in subsequent studies to develop relationships between reflectance indices and slowly changing canopy properties. The spectra are measured at a relatively high frequency (over sampling) compared to expected changes in canopy physiological properties, and thus, we can be quite selective in choosing data for analysis.

Examples of normalized irradiance and reflected radiance spectra at 1400 h for a sunny day and a cloudy day in summer are shown in Fig. 3. The irradiance and radiance spectra were normalized using the peak value of irradiance at 582–586 nm, since the calibration described in Section 3 applies only to the reflectance spectra. The reflected radiance spectra were measured at all four azimuths, although only three are shown for clarity in Fig. 3a and b. Cloud cover did not substantially affect the shape and magnitude of the normalized irradiance spectra, except for minor changes in amplitude between 750 and 780 nm. In contrast, the whole normalized reflected radiance spectrum was affected significantly by cloud cover when the periscope was facing south (away from the sun, Fig. 3b, c), with the normalized radiance on the sunny day being 0.24 units higher at 754 nm compared to the cloudy day. Radiances were higher in the visible waveband for the east-facing directions for clear skies than for overcast conditions and vice versa for the north-facing direction. There was little change in radiance for the westerly view direction (Fig. 3c). Clearly, individual radiance spectra depend on both BRDF effects and the ratio of diffuse to direct beam radiation. The MAS offers the opportunity to test whether radiation transfer models can remove these factors before the spectra are used to quantify canopy properties such as radiation use efficiency or when calculating reflectance indices. Spectra obtained with the MAS can also be used to test the sensitivity of reflectance indices to multiple view angles and both these aspects are discussed below.

The K95 model was used to assess the effect of incident solar and viewing geometry on the reflectance spectra. This model has been used to assess vegetation characteristics over large areas through model inversion (e.g., Bicheron & Leroy, 1999; Kuusk, 1998). The K95 model takes an analytical turbid medium approach to describe canopy reflectance in terms of leaf-level biochemical and canopy structural properties. Leaves

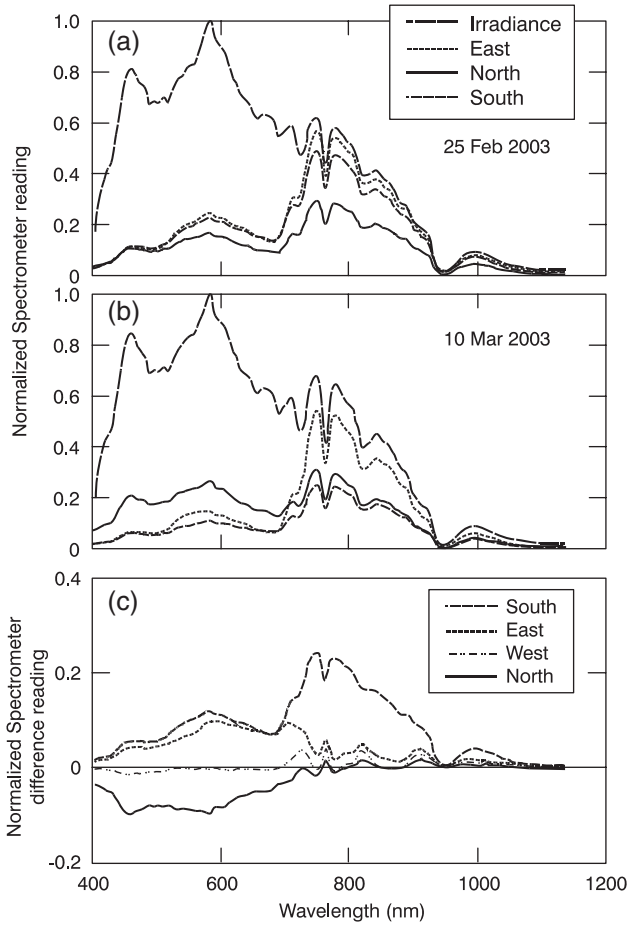

Fig. 3. Two examples of normalized irradiance and radiance spectra at 1400 h for three azimuths (E, N, and S) obtained from the MAS mounted above a forest canopy for (a) a sunny day, incoming solar radiation 660 W m^{-2} and (b) a cloudy day, incoming solar radiation 368 W m^{-2}. For clarity, the reflectance spectrum for the westerly azimuth is not shown in these two panels. (c) Difference radiance spectra (sunny–cloudy) for all four azimuths.

are assumed to be the principal scattering and absorbing elements in the medium and they are considered to be randomly located within the canopy and oriented according to a specified leaf angle distribution function. The optical properties of the leaves are described by their reflectance and transmittance spectra, while the properties of the background to the medium are described by the soil reflectance spectra. This approach has several advantages in theory (Bicheron & Leroy, 1999): it is simple, it provides a physically sound representation of the surface properties (soil plus vegetation) and may be more versatile than locally calibrated empirical models. The relative simplicity of the model allows it to be inverted to solve for key vegetative properties, such as leaf area index. Data from the MAS for a real forest can be used to test this model, as well as others of varying complexity, ranging from empirical indices to geometric-optical models of radiation transfer in plant canopies.

A representative soil reflectance spectrum required for the K95 model was calculated from the mean spectrum of three individual pixels of a high resolution HyMap image in an open area of exposed soil at the Tumbarumba site. Spectral images were obtained in March 2000 using the HyMap, 126-band airborne system, with a wavelength range 450–2500 nm and band widths between 15 and 20 nm (Hill et al., 2006-this issue). The spectral coverage is contiguous except for the regions where the atmosphere is opaque due to strong water vapor absorption (Cocks et al., 1998). Flight lines were oriented parallel to the solar principal plane to minimize the effects of variations in target directional reflectance and to cover the study area efficiently. Imagery was obtained under clear sky conditions with solar zenith angles between 40.3° and 40.6°, and at a nominal ground spatial resolution of 3 m. Data were converted to radiance using Integrated Spectronics software (Cocks et al., 1998). The ACORN Atmospheric correction program (version 3.12, Miller, 2002) was used to correct the imagery for atmospheric effects and the swaths were rectified to Australian Map Grid (AMG) coordinate systems to within 10 m accuracy.

Leaf level spectra for *Eucalyptus delegatensis* leaves grown under similar conditions were acquired using an ASD spectro-radiometer with integrating sphere in late spring 2001, allowing measurement of both reflectance and transmittance of the leaves. These spectral observations were input directly into the K95 model. Additional inputs parameters for the model are listed in Table 2.

Spectral reflectances predicted by the K95 model are compared to spectra measured at 0900 h and at 1600 h during summer in Fig. 4. Reflectance spectra in the visible region fall between 0.02 and 0.05 according to the model whereas the measured spectra lie between 0.03 and 0.10. Measured spectra in the visible waveband are more sensitive to azimuth than predicted by the model and this tendency is accentuated in the NIR region, particularly for the south direction (S) spectrum between morning and afternoon. The discrepancy between the modeled and the observed S spectrum may be due to a gap in the forest canopy in that direction, but a similar explanation does not apply to the other azimuths, where there were no large gaps in the canopy. Modeled and measured reflectances in the visible region are lower in summer than in winter (cf. Figs. 4 and 5), consistent with the lower sun elevation angle in winter. According to the model, winter reflectance spectra are less sensitive to azimuth than is observed in both the visible and NIR

Table 2
Parameters used in the Kuusk (1995) Model

Variable	Value
Canopy parameters	
Leaf to canopy height	0.5
Leaf clumping	0.5
Leaf angle distribution	90
Leaf angle distribution eccentricity	0.5
Leaf wax	1.0
Canopy leaf area index	1.2
Angstrom exponent (atmospheric parameter)	0.1
Soil zenith angle	0.0
Viewing parameters	
Solar zenith	Variable
Solar azimuth	Variable
View direction	See Table 1

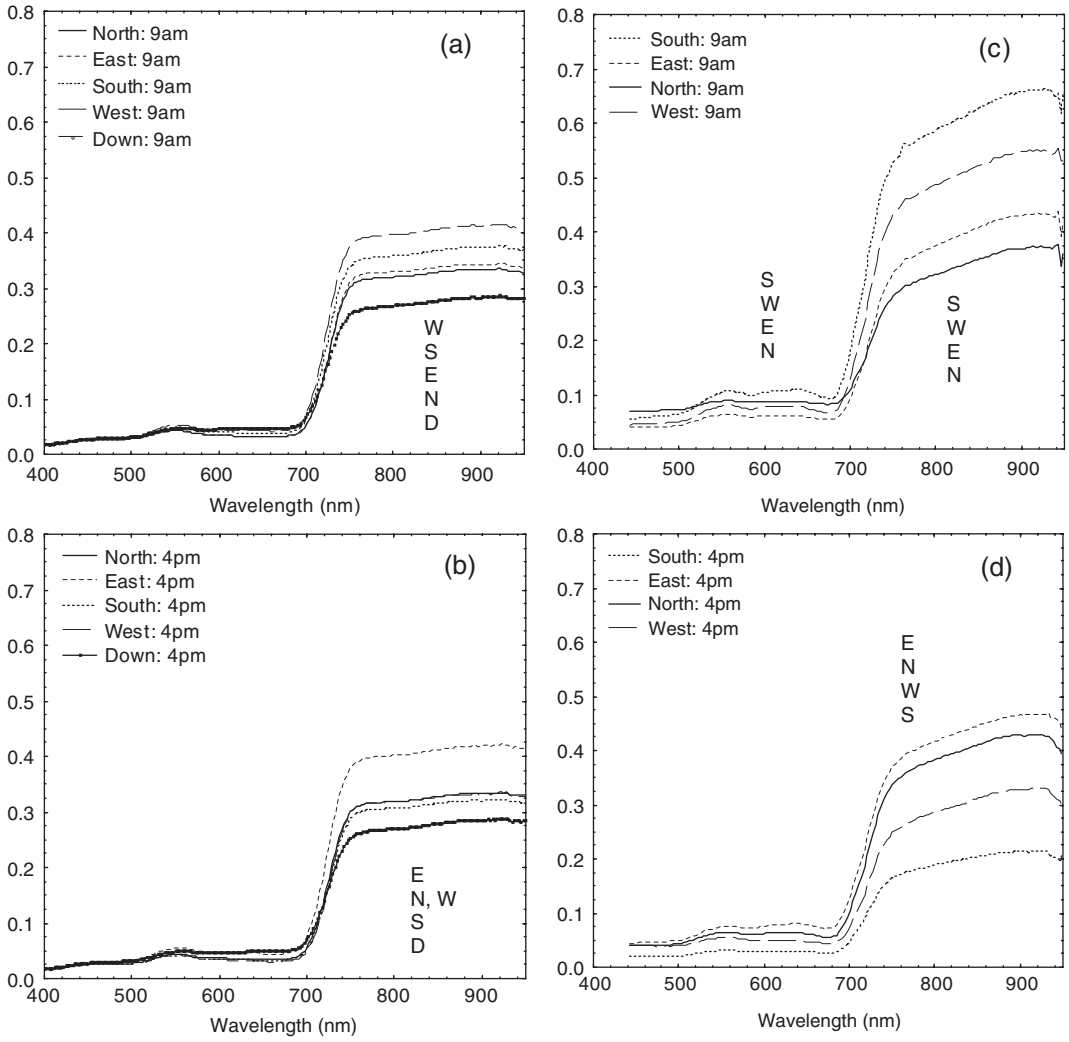

Fig. 4. Comparison of reflectance spectra calculated for four azimuths using the Kuusk (1995) model at (a) 9:00 AM and at (b) 4:00 PM on 26th February (austral summer) and measured spectra from the MAS (c and d). The order of the spectra in the visible and NIR is identified according to viewing direction, and the spectrum labeled 'down' or 'D' is from model predictions for a nadir-viewing radiometer.

wavebands (Fig. 5). Excluding the anomalous 'S' spectrum, the model predicts NIR reflectances of ~0.3 in the morning and afternoon whereas the observed reflectances were ~0.15 in the morning and between 0.3 and 0.4 in the afternoon. Figs. 4 and 5 show that closest agreement between observations and the model is for the north direction (N) spectrum in both the visible and NIR.

It is apparent that the K95 model, with its relatively simple assumption of radiation absorption by a uniform, turbid medium consisting entirely of leaves, provides only an approximate description of the near-field reflectance spectra observed over a *Eucalyptus* forest canopy. These discrepancies are undoubtedly due to the relatively open nature of the forest and because individual crowns are seen by the optical system, even at a zenith viewing angle of 58°. The K95 model does capture some of the variation in the observed spectra and its relative simplicity means that only a small number of parameters are required for the model. This is in contrast to geometric-optical models which involve more parameters and detailed descriptions of forest canopy structure but which may provide a better fit to the measurements than the simple models. Comparison of various models is warranted to resolve these issues and the MAS should prove useful in providing data to test the models.

The position of the spectrometer optics relative to the sun clearly affects the observed reflectance spectrum. It is possible to invert canopy radiative transfer models to solve for various canopy and leaf properties (e.g., Bicheron & Leroy, 1999), but the problem is often poorly constrained mathematically, resulting in imprecise estimates of model parameters (Myneni et al., 1995; Qiu et al., 1998). An alternative to inverting physical radiative transfer models is to use empirical reflectance indices, such as those summarized by Zarco-Tejada et al. (2001) and by Sims & Gamon (2002), to develop relationships between reflectances and various canopy properties. Examples include Carter (1998), who systematically explored relationships between photosynthetic capacity and a range of reflectance indices for plant canopies, and Zarco-Tejada et al. (2001) who made a similar study for leaf chlorophyll content. Hill et al. (2006-this issue) used various reflectance indices obtained using the MAS and several other remote-sensing systems to

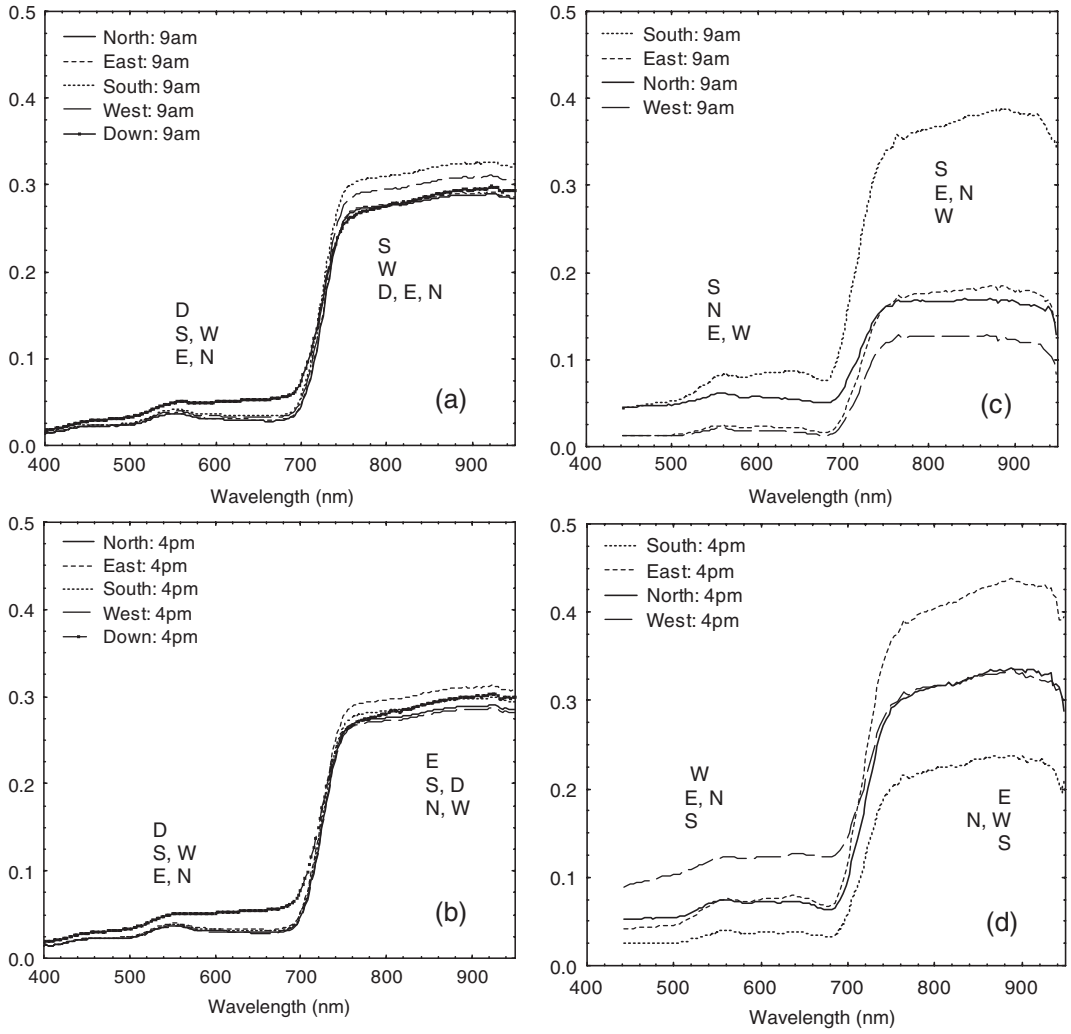

Fig. 5. Comparison of reflectance spectra calculated for four azimuths using the Kuusk (1995) model at (a) 9:00 AM and at (b) 4:00 PM on 31st July (austral winter) and measured spectra from the MAS (c and d). The order of the spectra in the visible and NIR are identified according to viewing direction, and the spectrum labeled 'down' or 'D' is from model predictions for a nadir-viewing radiometer.

develop relationships between CO_2 fluxes measured at the Tumbarumba flux tower. The influence of azimuth on these indices is rarely studied and hence is poorly understood.

As an initial exploration of these azimuthal effects, we used data from the MAS at Tumbarumba to examine the directional variation of three commonly used reflectance indices (Fig. 6): the normalized difference vegetation index (NDVI=$(R_{800}-R_{680})/(R_{800}+R_{680})$), the water-band index (WBI=R_{900}/R_{970}, Peñuelas et al., 1993) and the photochemical reflectance index (PRI=$(R_{570}-R_{531})/(R_{570}+R_{531})$, Gamon et al., 1997). Also shown are the same reflectance indices calculated using the K95 model at the four look angles of the MAS. The mean and standard deviation of the WBI (mean=1.092, S.D.=0.018) from the MAS are slightly greater than from the K95 model (mean 1.037, S.D.=0.010), and both show little variation with view direction. NDVI from the K95 model also shows little variation with view azimuth (mean=0.835, S.D.=0.003), compared to the lower mean and greater variability from the measurements (mean=0.685, S.D.=0.068). Modeled nadir-view values for both the WBI (1.023) and the NDVI (0.784)

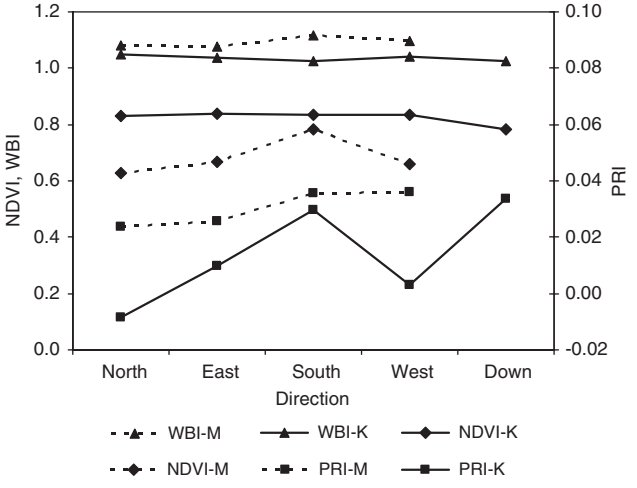

Fig. 6. Directional variation of three spectral indexes, NDVI, WBI and PRI at 1200 h on 10th March 2004. Dashed lines are measurements and solid lines are indices calculated using the K95 model. The points labeled 'Down' are calculated using the K95 model for a nadir look angle. Note that PRI from the K95 model has a negative value for the northerly view direction.

are slightly lower than the means calculated by the model for the four look angles used with the MAS. Mean values of the PRI are small (<0.04) and the variability with view direction from the MAS (S.D. = 0.0065) is half that from the K95 model (S.D. = 0.0160). The latter yields negative values for the northerly view direction, in contrast to positive values derived from the measurements. The PRI calculated for the nadir view with the K95 model (0.033) is greater than those calculated for the four other look angles and is similar to the mean of the PRI obtained with the MAS (0.030). Gamon et al. (1997) obtained negative PRI values from potted and field-grown plants and was able to use the PRI to distinguish between the photosynthetic activity of annual, deciduous and evergreen plants and between plants grown under differing nutrition. In contrast, Gamon et al. (1992) measured positive PRI values soon after removal of shading from sunflower leaves. These findings suggest that further work is needed to separate directional reflectance effects on the PRI from those due to variation in photosynthetic activity.

5. Conclusions

This paper presents technical details of the design, calibration and operation of a rotating optical periscope and spectrometer used to automatically measure the spectral reflectance of a forest canopy at multiple azimuths. Examples of irradiance and reflectance spectra are presented for the early afternoon during summer for a sunny and a cloudy day. Compared to clear skies around noon, overcast conditions altered the reflectance spectrum in the visible waveband for the east and north facing directions and increased the reflectance across both the visible and the NIR for the south view (away from the sun). Significant discrepancies were observed between the measured reflectance spectra and the canopy reflectance model of Kuusk (1995). These differences are likely due to the inhomogeneous nature of the forest canopy not satisfying the assumptions of a homogeneous turbid medium used in the K95 model. Despite these difficulties, reflectance indices calculated using the K95 for a nadir-view gave similar values to the mean of indices obtained with the MAS viewing the canopy at four azimuths. Measurements using the MAS can be used to investigate the directional dependence of several key reflectance indices and BRDF models will be useful in separating geometrical and physiological effects in the reflectance signals. The MAS system provides an ideal tool for such tests.

Acknowledgements

Thanks are due to the following people for making this project possible: Drs. Helen Cleugh and Alex Held for their support, ideas and advice, and Mr. Steve Zegelin and Mark Kitchen for their assistance during the installation of the system at the field site. Dr. Bisun Datt provided the spectra of the *E. delegatensis* foliage and the CSIRO Earth Observation Centre provided funds for HYMAP image acquisition Components of the Kuusk modelling were undertaken as part of GN's PhD thesis.

References

Baldocchi, D. D., Falge, E., Gu, L. H., Olson, R., Hollinger, D., Running, S., et al. (2001). FLUXNET: A new tool to study the temporal and spatial variability of ecosystem-scale carbon dioxide, water vapour and energy flux densities. *Bulletin of the American Meteorological Society*, *82*, 2415–2434.

Bicheron, P., & Leroy, M. (1999). A method of biophysical parameter retrieval at global scale by inversion of a vegetation reflectance model. *Remote Sensing of Environment*, *67*, 251–266.

Boegh, E., Soegaard, H., Broge, N., Hasager, C. B., Jensen, N. O., Schelde, K., et al. (2002). Airborne multispectral data for quantifying leaf area index, nitrogen concentration, and photosynthetic capacity in agriculture. *Remote Sensing of Environment*, *81*, 179–193.

Carter, G. A. (1998). Reflectance wavebands and indices for remote estimation of photosynthesis and stomatal conductance in pine canopies. *Remote Sensing of Environment*, *63*, 61–72.

Cocks, T., Jenssen, R., Stewart, A., Wilson, I., & Shields, T. (1998). The HyMap airborne hyperspectral sensor: The system, calibration and performance. In M. Schaepman, D. Schlapfer, & K. I. Itten (Eds.), *Proc. 1st EARSeL workshop on imaging spectroscopy, 6–8 October 1998, Zurich* (pp. 37–42). Paris: EARSeL.

Gamon, J. (2006). Spectral network (SpecNet)-what is it and why do we need it? *Remote Sensing of Environment*, *103*, 227–235 (this issue). doi:10.1016/j.rse.2006.04.003.

Gamon, J. A., Field, C. B., Fredeen, A. L., & Thayer, S. (2001). Assessing photosynthetic downregulation in sunflower stands with an optically-based model. *Photosynthesis Research*, *67*, 113–125.

Gamon, J. A., Penuelas, J., & Field, C. B. (1992). A narrow-waveband spectral index that tracks diurnal changes in photosynthetic efficiency. *Remote Sensing of Environment*, *41*, 35–44.

Gamon, J. A., Serrano, L., & Surfus, J. S. (1997). The photochemical reflectance index: An optical indicator of photosynthetic radiation use efficiency across species, functional types and nutrient levels. *Oecologia*, *112*, 492–501.

Goward, S. N., Cruickshanks, G. D., & Hope, A. S. (1985). Observed relation between thermal emission and reflected spectral radiance of a complex vegetated landscape. *Remote Sensing of Environment*, *18*, 137–146.

Hanan, N. P., Prince, S. D., & Begue, A. (1995). Estimation of absorbed photosynthetically active radiation and vegetation net production efficiency using satellite data. *Agricultural and Forest Meteorology*, *76*, 259–276.

Hill, M., Held, A., Leuning, R., Coops, N. C., Hughes, D., & Cleugh, H. A. (2006). MODIS spectral signals at a flux tower site: Relationships with high-resolution data, and CO_2 flux and light use efficiency measurements. *Remote Sensing of Environment*, *103*, 351–368 (this issue). doi:10.1016/j.rse.2006.06.015.

Hughes, D., Daniel, P., Kitchen, M., & Leuning, R. (2004). A multi-angle spectrometer for measuring plant canopy reflectance. *CSIRO Atmospheric Research Technical Report* No. xx., 21 pp.

Kuusk, A. (1995). A fast, invertible canopy reflectance model. *Remote Sensing of Environment*, *51*, 342–350.

Kuusk, A. (1998). Monitoring of vegetation parameters on large areas by the inversion of a canopy reflectance model. *International Journal of Remote Sensing*, *19*, 2893–2905.

Lang, A. R. G. (1986). Leaf area and average leaf angle from transmission of direct sunlight. *Australian Journal of Botany*, *34*, 349–355.

Lang, A. R. G. (1987). Simplified estimate of leaf area index from transmittance of the sun's beam. *Agricultural and Forest Meteorology*, *41*, 179–186.

Leuning, R., Cleugh, H. A., Zegelin, S., & Hughes, D. (2005). Carbon and water cycles in two contrasting Australian ecosystems: Wet/dry savannas and cool temperate *Eucalyptus* forest. *Agricultural and Forest Meteorology*, *129*, 151–173.

Miller, C. J. (2002). Performance assessment of ACORN atmospheric correction algorithm. *Algorithms and technologies for multispectral, hyperspectral, and ultraspectral imagery VIII; Aerosense 2002.* Orlando, FL: SPIE.

Monteith, J. L. (1977). Climate and the efficiency of crop production in Britain. *Philosophical Transactions of the Royal Society of London. Series B, Biological Sciences*, *281*, 277–294.

Myneni, R. B., Maggion, S., Iaquinto, J., Privette, J. L., Gobron, N., Pinty, B., et al. (1995). Optical remote-sensing of vegetation—modeling, caveats, and algorithms. *Remote Sensing of Environment*, *51*, 169–188.

Pearlman, J. S., Barry, P. S., Segal, C. C., Shepanski, J., Beiso, D., & Carman, S. L. (2003). Hyperion, a space-based imaging spectrometer. *IEEE Transactions on Geoscience and Remote Sensing*, *41*, 1160–1173.

Peñuelas, J., Filella, I., Biel, C., Serrano, L., & Save, R. (1993). The reflectance at the 950–970 nm region as an indicator of plant water status. *International Journal of Remote Sensing*, *14*, 1887–1905.

Peñuelas, J., Filella, I., & Gamon, J. A. (1995). Assessment of photosynthetic radiation-use efficiency with spectral reflectance. *New Phytologist*, *131*, 291–296.

Prince, S. D. (1991). Satellite remote-sensing of primary production—comparison of results for Sahelian grasslands 1981–1988. *International Journal of Remote Sensing*, *12*, 1301–1311.

Qiu, J., Gao, W., & Lesht, B. M. (1998). Inverting optical reflectance to estimate surface properties of vegetation canopies. *International Journal of Remote Sensing*, *19*, 641–656.

Running, S. W., Baldocchi, D. D., Turner, D. P., Gower, S. T., Bakwin, P. S., & Hibbard, K. A. (1999). A global terrestrial monitoring network integrating tower fluxes, flask sampling, ecosystem modeling and EOS satellite data. *Remote Sensing of Environment*, *70*, 108–127.

Sellers, P. J., Berry, J. A., Collatz, G. J., Field, C. B., & Hall, F. G. (1992). Canopy reflectance, photosynthesis and transpiration. III. A reanalysis using improved leaf models and a new canopy integration scheme. *Remote Sensing of Environment*, *42*, 187–216.

Sims, D. A., & Gamon, J. A. (2002). Relationships between leaf pigment content and spectral reflectances across a wide range of species, leaf structures and developmental stages. *Remote Sensing of Environment*, *81*, 337–354.

Wang, Y. P., Leuning, R., Cleugh, H., & Coppin, A. (2001). Parameter estimation in surface exchange models using non-linear inversion: How many parameters can we estimate and which measurements are most useful? *Global Change Biology*, *7*, 495–510.

Waring, R. H., Law, B. E., Goulden, M. L., Bassow, S. L., Mccreight, R. W., Wofsy, S. C., et al. (1995). Scaling gross ecosystem production at harvard forest with remote-sensing—a comparison of estimates from a constrained quantum-use efficiency model and eddy-correlation. *Plant, Cell and Environment*, *18*, 1201–1213.

Warren Wilson, J. (1960). Estimation of foliage denseness and foliage angle by inclined point quadrats. *Australian Journal of Botany*, *11*, 95–105.

Zarco-Tejada, P. J., Miller, J. R., Noland, T. L., Mohammed, G. H., & Sampson, P. H. (2001). Scaling-up and model inversion methods with narrowband optical indices for chlorophyll content estimation in closed forest canopies with hyperspectral data. *IEEE Transactions on Geoscience and Remote Sensing*, *39*, 1491–1507.